Institut de Physique Nucléaire de Lyon

Université Claude Bernard

IN2P3 - CNRS

LYCEN 2000/29
March 2000

Excitation energy of the fragments produced in central collisions of Xe + Sn at intermediate energies

S. Hudan, et al., INDRA Collaboration

XXXVIII[th] International Winter Meeting on Nuclear Physics – Bormio – January 17-21, 2000

43, Boulevard du 11 Novembre 1918 - 69622 VILLEURBANNE Cedex - France

Excitation energy of the fragments produced in central collisions of Xe + Sn at intermediate energies.

S. Hudan[1], A. Chbihi[1], J.D. Frankland[1], J.P. Wieleczko[1], G. Auger[1], Ch.O. Bacri[2], N. Bellaize[3], F. Bocage[3], B. Borderie[2], R. Bougault[3], B. Bouriquet[1], R. Brou[3], P. Buchet[4], J.L. Charvet[4], J. Colin[3], D. Cussol[3], R. Dayras[4], A. Demeyer[5], D. Doré[4], D. Durand[3], E. Galichet[2,8], E. Genouin-Duhamel[3], E. Gerlic[5], D. Guinet[5], P. Lautesse[5], F. Lavaud[2], J.L. Laville[1], J.F. Lecolley[3], C. Leduc[5], R. Legrain[4], N. Le Neindre[3], O. Lopez[3], M. Louvel[3], A.M. Maskay[5], L. Nalpas[4], J. Normand[3], M. Pârlog[6], J. Péter[3], E. Plagnol[2], M.F. Rivet[2] E. Rosato[7], F. Saint-Laurent[1a], J.C. Steckmeyer[3], M. Stern[5], G. Tăbăcaru[6], B. Tamain[3], L. Tassan-Got[2], O. Tirel[1], E. Vient[3], C. Volant[4]
(INDRA collaboration)

[1] GANIL, CEA et IN2P3-CNRS, B.P. 5027, F-14076 Caen Cedex, France.
[2] Institut de Physique Nucléaire, IN2P3-CNRS, F-91406 Orsay Cedex, France.
[3] LPC, IN2P3-CNRS, ISMRA et Université, F-14050 Caen Cedex, France.
[4] DAPNIA/SPhN, CEA/Saclay, F-91191 Gif sur Yvette Cedex, France.
[5] Institut de Physique Nucléaire, IN2P3-CNRS et Université, F-69622 Villeurbanne Cedex, France.
[6] National Institute for Physics and Nuclear Engineering, RO-76900 Bucharest-Măgurele, Romania.
[7] Dipartimento di Scienze Fisiche e Sezione INFN, Università di Napoli "Federico II", I-80126 Napoli, Italy.
[8] Conservatoire National des Arts et Métiers, F-75141 Paris cedex 03.
a) present address: DRFC/STEP, CEA/Cadarache, F-13018 Saint-Paul-lez-Durance Cedex, France

---

Abstract

Experimental characteristics of the primary fragments produced in central collisions of Xe + Sn system from 32 to 50 AMeV have been deduced. By using the relative velocity correlation technique between the light charged particles (LCP) and detected fragments, we were able to extract the multiplicities and average kinetic energy of the associated secondary evaporated LCP. We then reconstructed the size and excitation energy of the primary fragments. For each bombarding energy a constant value, in MeV per nucleon, over the whole range of fragment charge has been found, suggesting that on the average thermodynamical equilibrium has been achieved at the freeze-out. This value increases slightly from 2.8 to 3.8 AMeV with a large increase of bombarding energy, 32 to 50 AMeV.

1 Introduction

The experimental reconstruction of the freeze-out configuration, a concept assumed in some statistical models [1–5], is one of the most fascinating challenges in the understanding of the nuclear multifragmentation processes [6–8]. It may allow us to go a step back in time closer to the early stages of the reaction. The comparison between data and multifragmentation phenomenological models [9–15] is then more direct. In particular, the hybrid models which marry dynamical and statistical aspects might be avoided. A recent experimental work[16] has shown that the reconstruction of the size and excitation energy of the primary fragments, at the freeze-out, was possible by means of fragment-light charged particles (IMF-LCP) correlation functions. A constant value of the excitation energy of the primary fragments has been deduced around 3 AMeV, suggesting that thermodynamical equilibrium has been achieved at the freeze-out.

In this contribution we extend the previous study[16] to a wider incident energy range, from 32 to 50 AMeV for central collisions of the Xe + Sn system measured with the 4π INDRA detector[17,18]. Excitation functions for the fragment excitation energy and the fraction of secondary emitted LCP correlated to the fragments will be shown. After a brief description of the detector and the event selection in section 2, we will describe in section 3 the method employed to extract the LCP's correlated to each fragment. The method used in this work is different from the previous one[16]. The experimental results are then given in section 4 and discussed in section 5.

2 Experiment

2.1 Experiment set-up description

The experiment was performed at GANIL with the multidetector INDRA [17,18]. This charged product detector covers about 90% of the 4π solid angle. The total number of detection cells is 336 arranged according to 17 rings centered on the beam axis. The first ring (2°-3°) is made of fast NE102/NE115 phoswich detectors. Rings 2 to 9 cover the angular range from 3° to 45° and are made of three detector layers : a low pressure gas-ionization chamber, a 300 μm thick silicon detector and a 14 to 10 cm thick CsI(Tl) scintillator. The remaining 8 rings cover the angular range from 45° to 176° and have two

detection layers : ionization chamber and 7.6 to 5 cm thick CsI(Tl) scintillator. For the studied system Xe + Sn, fragments with Z up to 54 are identified in the forward region. Beyond 45°, the ion identification is obtained up to Z=16. Over the whole angular range, a very good isotope identification is obtained for Z=1 to Z=3, except for particles with low energies where ambiguities are unresolved.

The energy calibration of the CsI(Tl) scintillators was obtained for light charged particles (LCP) by means of the elastic and inelastic scattering of secondary LCP beams ($p, d, t, ^3He, ^4He$) produced by the fragmentation of a 95 AMeV ^{16}O beam in a thick C target. These particles were then momentum selected by the "alpha magnetic spectrometer" and scattered in a C or Ta target installed in the INDRA reaction chamber. For $Z \geq 3$ fragments, the energy calibration was made by using the $\Delta E/E$ technique. A typical energy resolution was about 4%. The energy threshold was a few 100 keV for light particles, 0.7 AMeV for Z=3 and 1.4 AMeV for Z=35. A complete technical description of INDRA, its calibration and its electronics can be found in [17,18].

2.2 Event selection

Two selections have been made to isolate central collisions. The first one is the requirement of quasi-complete events by accepting in the off-line analysis only events having total detected charge (Z_{tot}) $\geq$ 80% of the initial total charge of the system. The second is the use of the flow angle, (θ_{flow}) selection[19–21]. This angle is a global observable defined as the angle between the beam direction and the main axis of the event shape. For spherical event the flow angle is not any more defined and can take all values between 0 and 90°. In the opposite, for elongated event shape it takes low values. Therefore we defined the central collisions as the quasi-complete events having $\theta_{flow} \geq 45°$ for high bombarding energies and $\theta_{flow} \geq 60°$ for the 32 AMeV system.

3 Correlation functions

One of the scenario proposed to explain the multifragmentation process is suggested by certain microscopic transport codes and may be invoked as a basis for the successful statistical models. Semi-classical one-body calculations [11–13] indicate for example that in central collisions around the Fermi energy (25-50 AMeV) the colliding nuclei can form a hot and dense compact system, which then expands towards low densities. The system is then in the spinodal region, where small fluctuations can produce the fragments. Those fragments

can be excited and they may decay by emitting light particles (LP). However during the whole process LP can be emitted : as preequilibrium in the first stages of the collision, during the expansion phase, at the freeze-out and finally as secondary decay of the formed fragments. Going back to the freeze-out volume assumes that we are able experimentally to isolate the secondary contribution. This is possible if the formed fragment at the freeze-out are no too excited so that the time scale associated to their decay is much greater than the time scale of their production.

Correlation functions are a powerful tool for extracting small signals. This is the method we used to extract, on the average, the LCP emitted from each fragment. With the help of simulations we have developed a correlation technique to extract possible signals.

3.1 Simulation of the background shape

We used a modified version of the SIMON event generator [22] to simulate the scenario inspired by BNV [13]calculations. Two steps are assumed in these simulations. The first step is the cooling of the initial fused system through a sequential LP emission process, the second one is the fragmentation of the smaller remaining source where the remaining excitation energy is shared between a fixed number of primary fragments (typically 6 to 7 fragments). Then the primary fragments decay sequentially while moving apart under Coulomb forces plus an initial radial velocity. This simulation reproduces reasonably well the global experimental features. In particular the kinematical observables are well reproduced.

The calculated relative velocity are shown in fig.1.a (thick lines) for Ne-p pairs and for a beam energy of 50AMeV. In the same figure are plotted different contributions : the primary contribution (dotted histogram), the evaporated protons from all other fragments except the neon (dot-dashed histogram) and finally the protons emitted from the parents of detected neon fragment (hatched-dashed histogram). As expected, the latter contribution is very small, it represents the protons truly correlated with a neon nucleus that we must extract from the data. Fig.1.b show the uncorrelated relative velocity for Ne-p pairs reconstructed by the event mixing procedure. For each neon found in an event having a number of proton N_p we take randomly N_p proton emitted from N_p other events. This technique is different from the one reported in ref.[16] where Li nuclei are used to decorrelate the events. The problem in the latter technique is that the Li can be the product of the known resonance ^7Be which decays to $^6Li + p$ and increases the background, thus decreasing the yield of true correlated protons. Fig.1.c. and 1.d. show the Ne-p correlation function and the difference function, respectively. In the same figures is plotted the

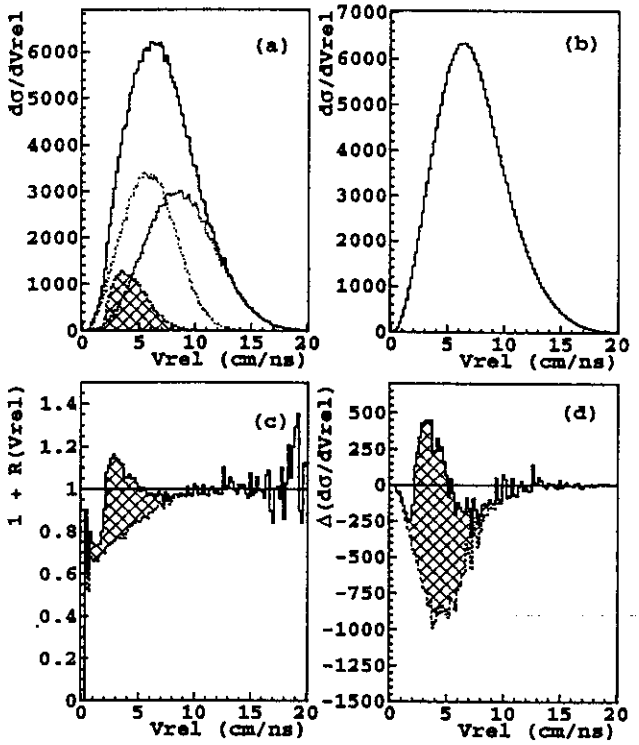

Fig. 1. Relative velocity spectra for simulated Ne-p pairs. (a)For correlated events. The total spectra (thick histogram) and different contributions are shown(see text). (b)For uncorrelated events. (c) The correlation function (continuous histogram), the real background (dashed histogram) and the contribution from the secondary emission from the parents of the Ne fragments (hatched area) are shown. (d) The difference function is shown here. The notations are similar to the picture (c).

associated true background (dashed histogram). The hatched areas represent the contribution of secondary emission from the parents of neon. The shape of the background has been nicely fitted by the function :

$$R(V_{rel}) = A - \frac{1}{BV_{rel} + C} \tag{1}$$

where A, B and C are parameters which differ for each fragment-LCP pair. In fact only 3 coordinates are needed to resolve this equation, we then used particular points to do so : the first one corresponds to the local minimum seen at the small relative velocity in the difference function (Fig.1.d.) which corresponds to the onset of the proton emission (or threshold), the second one corresponds to the first point where the difference function is equal to zero, just after the second minimum, in this region the secondary evaporation vanishes. The third one corresponds to the point where the correlation function (Fig. 1.c) goes to zero. The fact that the experimental shape of the correlation function as well as the difference function (Fig.2. upper panels) have the same behaviour, we applied this method to the experimental data to extract the

background. From this simulation and method developed above we are more confident to isolate the LCP evaporated from the primary fragment.

3.2 Application to the data

Fig. 2 shows the experimental correlation function, the difference function and the velocity distribution of protons correlated to neon fragments for the central collisions of Xe + Sn at 50 AMeV. In the same figure are plotted the corresponding background calculated with eq.1 by using three points taken from the experimental distributions as described in the above section. Therefore the proton velocity spectrum is deduced by subtracting the difference function from the corresponding background (the curve in fig 2. upper right panel).This distribution is obtained directly in the centre of mass of the neon fragment. It has a Maxwellian shape which verifies the validity of the method employed. From the mean value of the distribution we can deduce the average kinetic energy of protons. Its integral normalized to the total number of neons, provides the average multiplicity of protons evaporated from parents of Ne fragments.

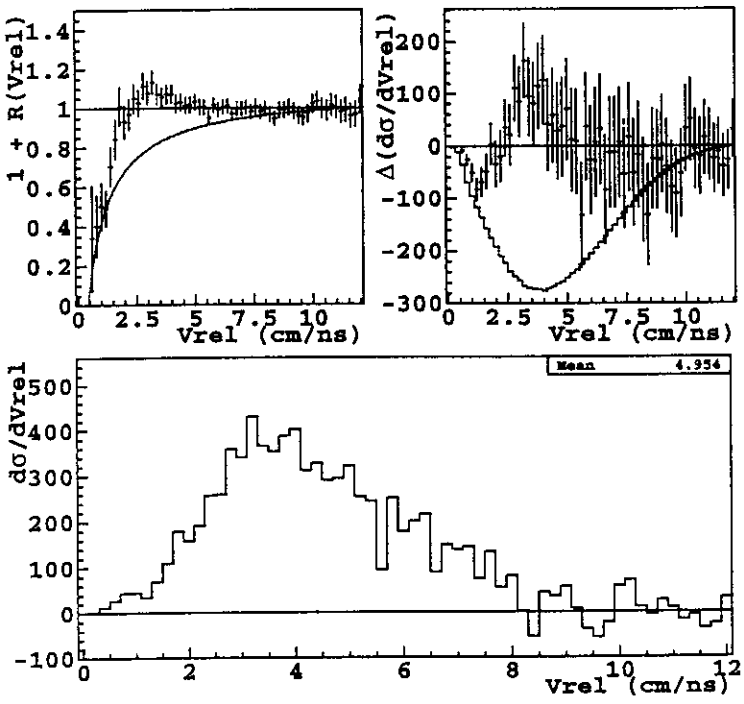

Fig. 2. For the data: In the upper panel are shown respectively the correlation function(left) and the difference function(right) for the protons correlated with the Neon. The corresponding velocity spectrum of protons in the centre of mass of the Neon fragment (lower panel) is shown.

4 Experimental results

4.1 Average multiplicities and kinetic energies of the LCP correlated to the fragments

We applied the method described above for the four measured systems and for all combinations of LCP isotopes and fragment pairs.

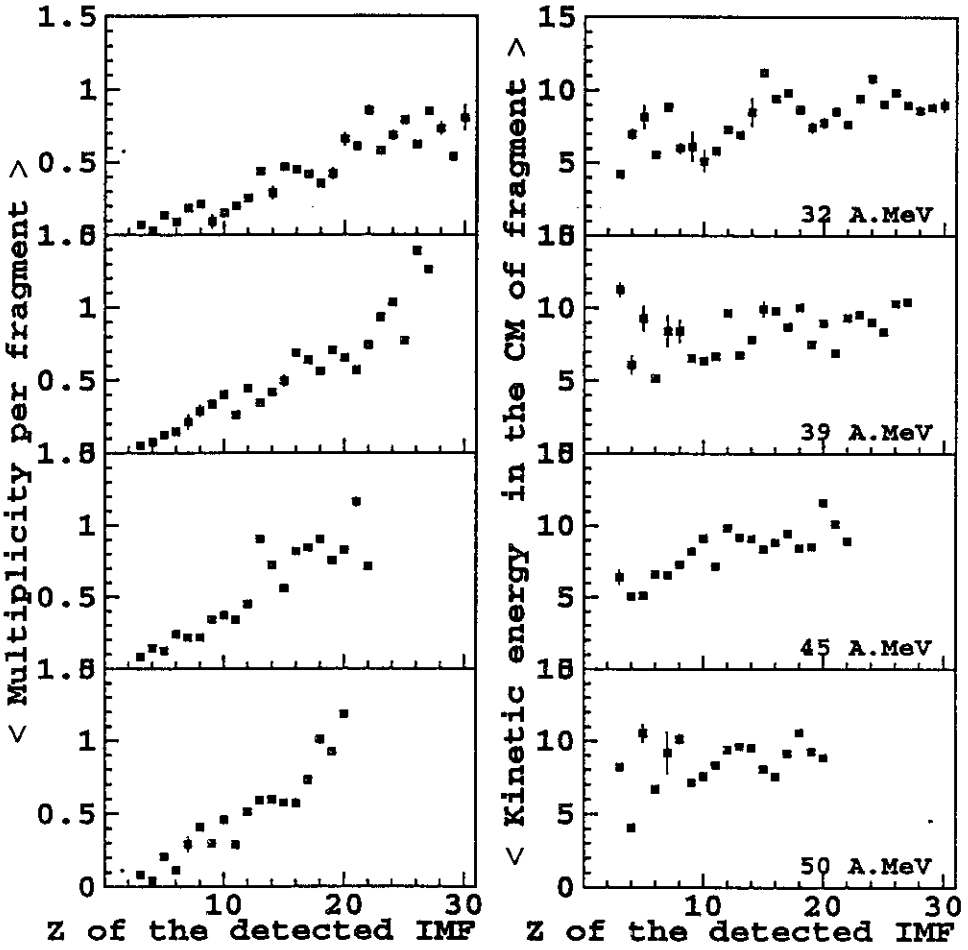

Fig. 3. For the data: Average secondary multiplicities per IMF of protons (left panel) and their average kinetic energy in the center of mass of the fragments (right panel) as a function of the charge of the detected fragments.

The extracted average proton multiplicities and their average kinetic energy in the CM of the fragment are given in figure 3 as a function of the charge, Z, of the detected fragments and for the four bombarding energies. The average multiplicities increase with the fragment size which suggests an increase of the

excitation energy of the primary fragments. These excitation energies must be small if we consider the low value obtained for the average multiplicities. They do not exceed a value of 1.8 even for the other particles (not shown here). The average kinetic energy also increases but slightly with the charge of the fragment. This behaviour might be due to the Coulomb barrier effect. It is worth noting that the multiplicity for a given fragment increases with the bombarding energy. Moreover we extract the multiplicities of $d, t, ^3He$, α and Li particles correlated to each fragment ranging from Z = 3 up to Z = 20-30 (not shown in this contribution). They exhibit the same behaviour and the same conclusions can be drawn.

4.2 Reconstruction of the size and excitation energy of the primary fragments

To reconstruct the charge of the primary fragments we used the LCP multiplicities correlated to each fragment as described in the last paragraph. Therefore the average charge of the primary fragment, $< Z_{pr} >$, is given by the sum of the detected fragment and all evaporated LCP's charge weighted by their corresponding multiplicities. $< Z_{pr} >$ is then given by the relationship :

$$< Z_{pr} >= Z_{IMF} + \sum z_i < M_i > \qquad (2)$$

where Z_{IMF} is the detected fragment charge, z_i and $< M_i >$ are the charge and the average multiplicity of the evaporated particle $i = p, d, t, ^3He, \alpha$ and Li.

The values of the primary charge obtained with this reconstruction vary from one charge to 7 charge units more than the detected fragment. For example $Z_{pr} = 25$ corresponding to the detected fragment $Z_{IMF} = 20$, and $< Z_{pr} >= 6$ when the detected fragment is $Z_{IMF} = 5$, for the 50AMeV bombarding energy.

In order to reconstruct the mass of the primary fragments, quantity needed to deduce the excitation energy, we made two extreme assumptions : the first one is that the primary fragments are produced in the valley of stability, the second assumes that they are produced with the same N/Z ratio as the composite initial system. However, as mentioned above the INDRA detector does not resolve the fragment isotopes, we therefore made an additional assumption which supposes that the detected fragments are in the valley of stability. In the framework of these assumptions we reconstruct the primary fragment masses and deduce the number of neutrons evaporated from the primary fragments.

At this stage, the calorimetric procedure can be applied to reconstruct the average excitation energy of the primary fragments ($< E^*_{pr} >$). Thus it is

given by the relationship :

$$< E^*_{pr} >= \sum < M_{LCP} >< E_{LCP} > + < M_n >< E_n > -Q \qquad (3)$$

where $< E_{LCP} >$ and $< E_n >$ are the average kinetic energies of the measured evaporated LCP's and the deduced neutrons with the average multiplicity $< M_n >$. Q is the corresponding mass balance of the reaction $A_{pr} - - - - > A_{IMF} + \sum a_i < M_i >$, where A_{pr}, A_{IMF} and a_i are respectively the masses of the primary fragment, the detected fragment and the associated evaporated LP including the neutrons.

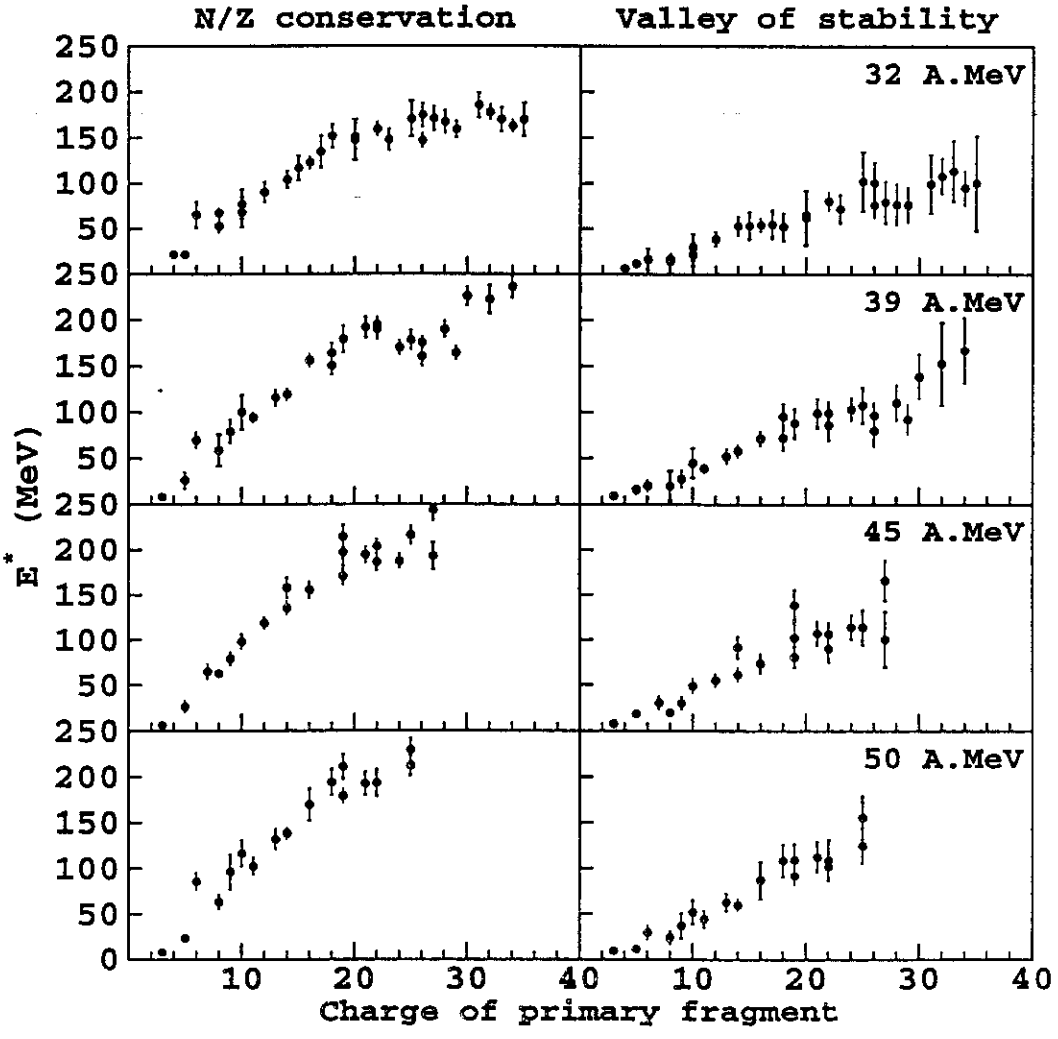

Fig. 4. Average excitation energy of the primary fragments as a function of their atomic number. Left panels:the primary fragments have the same N/Z as the combined system. Right panels:the fragments are produced in the valley of stability.

Fig. 4 shows the result of this procedure for the two senarii and at the four bombarding energies. As expected from the deduced multiplicities (see section 3.2), the excitation energy increases with the size of the primary fragment for all bombarding energies and for the two assumptions. However, for the 32 AMeV system, $< E^*_{pr} >$ seems to saturate at high charges which may be due to the limits of the method. We can give no physical explanation of this saturation. To decide which scenario can be kept the one assuming that the primary fragments are produced in the valley of stability or with N/Z conservated, extensive statistical calculations have been performed using the GEMINI[23] code, for the 50 AMeV system. In these calculations the input of the code were the experimental deduced primary charge, their masses with the two assumptions and their associated excitation energies. The comparison to the experimental LCP multiplicities and kinetic energies suggests that the N/Z assumption is the most reasonable scenario. Details of these calculations are given in ref.[16].

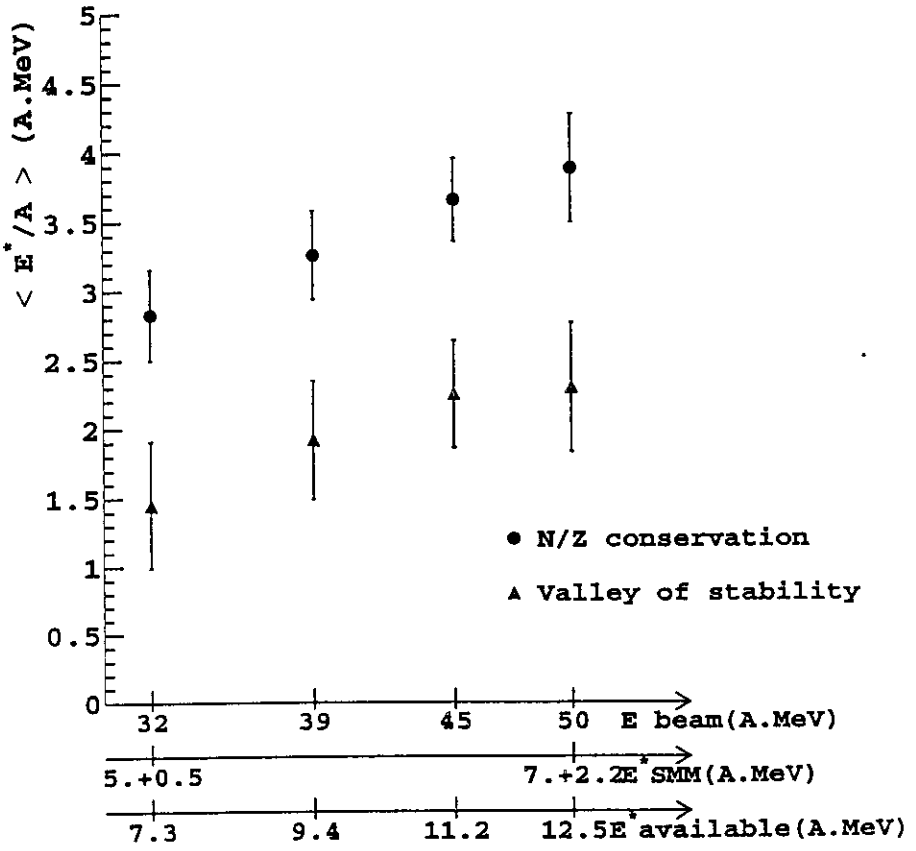

Fig. 5. Average excitation energy per nucleon of the primary fragments as a function of bombarding energy. The dots and the triangles correspond to the primary fragments having the same N/Z as the combined system, and produced in the valley of stability respectively.

The linear trend of the $< E^*_{pr} >$ with the primary charge indicates that the average excitation energy per nucleon, $< e^*_{pr} >$ in MeV/nucleon, is constant whatever the size of the primary fragment. We verified the latter characteristic by plotting this variable and we deduced a constant value for each bombarding energy. Figure 5 shows the evolution of this value obtained by averaging over the whole set of the associated primary fragments as a function of the bombarding energy. The vertical bars are the standard deviations from the mean values. They are small and do not exceed 1 AMeV, which support the constance of the value of $< e^*_{pr} >$. Therefore, the temperature of the primary fragments has a constant value which suggests that thermodynamical equilibrium has been achieved at all bombarding energies.

It is worth noting, that the excitation energy per nucleon increases slightly, only 1 AMeV, although the incident energy ranges from 32 to 50 AMeV. The corresponding available energy varies over a large domain, from 7.3 up to 12.5 AMeV. In terms of thermal energy, SMM calculations have been performed for these systems and reproduce the data for thermal energy of the initial source ranging from 5 to 7 AMeV. Details of these calculations can be found in ref.[24,25]. This slight increase of temperature with the thermal excitation energy of the source may indicate that the system is in the liquid-gas coexistence phase. However, other signals and studies dealing with the search for the phase transition are probably more appropriate to this purpose, see for instance refs. [26–28] and the contributions of M. D'Agostino et al., R. Bougault et al., to this conference.

It is interesting to give an estimate of the proportion of thermally (secondary) emitted LCP relative to the total LCP produced in the whole process. This proportion P is given by :

$$P = \frac{\sum M_{sec} M_{IMF}}{M_{tot}} \tag{4}$$

where M_{sec}, is the secondary LCP multiplicity per fragment, extracted by the method described above, weighted by the measured fragment multiplicity per event, M_{IMF}, and M_{tot} is the total multiplicity per event. This ratio decreases from 40% to 30% when the bombarding energy increases from 32 to 50 AMeV. This behavior can be interpreted as an increase of non equilibrium LCP emission with the bombarding energy. However this thermal component percentage is at its low limit. Other thermal like contributions produced at the freeze-out at the same time than the fragments or originating from the decay of unstable fragments[29] such as ^8Be, ^5Li etc. must be included.

5 Conclusion

In this work we extracted the experimental contribution of secondary LCP evaporated by the primary fragments produced in the central collisions of the Xe + Sn for four bombarding energies, 32, 39, 45 and 50 AMeV. Using the relative velocity correlation techniques, we were able to isolate the secondary velocity distribution of each LCP isotope correlated to each fragment. We then deduced the average multiplicity per fragment and kinetic energy of secondary LCP. Therefore we reconstruct the size and the excitation energy of the primary fragments produced at the freeze-out allowing us to go one step back in time closer to the early stages of the reaction. This new observable can provide significant constraint on different multifragmentation models. At a given beam energy the excitation energy per nucleon of the primary fragments is constant whatever the size of the primary fragment. This experimental finding is compatible with the assumption of thermodynamical equilibrium at the freeze-out time. The value of $< e^*_{pr} >$ (in MeV/nucleon) varies slightly from 2.8 to 3.8 A.MeV with a large increase of bombarding energy. It corresponds to a temperature of the primary fragment about 4-5 MeV. This value might be an upper limit of temperature that nuclei can sustain. We also deduced the proportion of secondary evaporated LCP to the total measured multiplicity, which varies from 40 to 30% with the bombarding energy. The remaining proportion of LCP are produced before and during the freeze-out.

References

[1] D.H.E. Gross Rep. Prog. Phys. **53** (1990) 605.

[2] J.P. Bondorf et al., Phys. Rep. **257** (1995) 133.

[3] A.S. Botvina et al., Nucl. Phys. **A475** (1987) 663.

[4] W.A. Friedman et al., Phys. Rev. Lett. **60** (1988) 2125.

[5] W.A. Friedman et al., Phys. Rev. **C42** (1990) 667.

[6] W. G. Lynch, Ann. Rev. Nuc. Sci. 37 (1987) 493.

[7] L. Moretto, G. Wozniak, Ann. Rev. Nuc. Sci. 43 (1993) 379.

[8] B. Tamain, D. Durand, Preprint LPCC 97-0???
(to be published in Proceedings of the Summer School Les Houches ed. H. Niffenecker (1997)).

[9] J. Aichelin et al., Phys. Rev. **C37** (1988) 2451

[10] A. Ono et al., Phys. Rev. Lett. **68** (1992) 2898

[11] Ph. Chomaz et al., Phys. Lett. **B254** (1991) 340

[12] M. Colonna et al., Phys. Rev. **C51** (1995) 2671.

[13] A. Bonasera et al., Phys. Rep. **243** (1994) 1.

[14] G.F. Bertsch and P.J. Siemens, Phys. Lett. **B126** (1983) 9.

[15] A. Guarnera et al., Phys. Lett. **B373** (1996) 267.

[16] N. Marie et al., Phys. Rev. **C58** (1998) 256.

[17] J. Pouthas et al., Nucl. Inst. and Meth. **A357** (1995) 418;

[18] J. Pouthas et al., Nucl. Inst. and Meth. **A369** (1996) 222

[19] J. Cugnon and D. L'Hôte, Nucl. Phys. **A397** (1983) 519.

[20] J.F. Lecolley et al, Phys. Lett. **B325** (1994) 317.

[21] N. Marie et al, Phys. Lett. **B391**, 15 (1997)

[22] D. Durand et al, Phys. Lett. **B345** (1995) 397

[23] R.J. Charity et al. Nucl. Phys. **A483** (1988) 371.

[24] R. Bougault et al., Proc. XXXVI Meeting on Nuclear Physics. Bormio, Italy, January 1997.

[25] S. Salou, PhD thesis, université de Caen, 1997.

[26] M. D'Agostino et al., Nucl. Phys. **A650** (1999) 329.

[27] Ph. Chomaz and F. Gulminelli, Nucl. Phys. **A647** (1999) 153.

[28] F. Gulminelli et al., submitted (1999).

[29] T. K. Nayak et al., Phys. Rev. **C45** (1992) 132.